Predicted Profiles of Ion Concentrations in Olfactory Cilia in the Steady State

Bernd Lindemann
Department of Physiology, Universität des Saarlandes, D-66421 Homburg, Germany

ABSTRACT The role of ciliary geometry for transduction events was explored by numerical simulation. The changes in intraciliary ion concentrations, suspected to occur during transduction, could thus be estimated. The case of a single excised cilium, having a uniform distribution of membrane channels, voltage clamped to −80 mV, was especially investigated. The axial profile of membrane voltage was that of a leaky cable. The Ca^{2+} concentration profile tended to show a maximum in proximal segments, due to a preponderance of Ca^{2+} inflow over Ca^{2+} export at those locations. The local increase in Ca^{2+} concentration activated Cl^- channels. The resulting current caused a local drop in Cl^- concentration, especially at the tip of the cilium and in distal segments, accompanied by a drop in ciliary K^+ concentration. In consequence, the membrane Cl^- current was low in distal segments but stronger in proximal segments, where resupply was sufficient. The model predicts that the Cl^- depletion will codetermine the time course of the receptor potential or current and the ciliary stimulus-response curve. In conclusion, when modeling with transduction elements presently known to participate, the ciliary geometry has large effects on ion distributions and transduction currents because ciliary ion transport is limited by axial electrodiffusion.

INTRODUCTION

Presently, there is increased interest in electrophysiological events occurring in subcellular compartments like dendrites and spines of neurons and transduction compartments like cilia, outer segments, and stereocilia. The small size of these membrane-bound structures (an olfactory cilium of the rat has a volume in the order of 0.2 fL only) will allow for large changes of ion concentrations in the interior. The resulting diffusion gradients in the "cytosol" codetermine the amplitude of the concentration changes. Despite the interest, only a few studies have dealt with the diffusion events in subcellular compartments in a quantitative and rigorous way (Qian and Sejnowski, 1989; Lumpkin and Hudspeth, 1998; Nygren and Halter, 1999). The present study takes the olfactory cilia as an example, where the equations for membrane transport and cytosolic diffusion of ions may be combined into an electrodiffusional cable formalism.

Sensory cilia of olfactory receptor cells are long and slender protrusions of the apical membrane. Their diameter is between 0.1 and 0.2 μm, and their length varies between 20 and 200 μm across vertebrate species (Lidow and Menco, 1984). This striking geometry is likely to be relevant to the transduction process. Although the cilia and similar structures have been scrutinized with respect to their electrical cable properties (Kaissling, 1971; Pongracz et al., 1991; Kleene et al., 1994; Larsson et al., 1997), the cable formalism used therein has assumed constant intraciliary concentrations. Thus, core ion gradients have been ignored. Presently it is unknown, therefore, to what extent ciliary volume and length may codetermine dynamic changes in ciliary ion concentrations and, thereby, affect time course and magnitude of the receptor currents.

To probe this question, software for simulation of olfactory cilia was developed. It solves the partial differential equations of simultaneous transport and diffusion of several ionic species numerically in the steady state, based on morphological and biophysical detail. Basic properties of the ciliary diffusion system could thus be explored as a first step toward a realistic simulation of olfactory transduction.

DESCRIPTION OF THE MODEL

The experimental paradigm adopted for the modeling was that of a single voltage-clamped cilium responding to odorants. Single cilia can be excised from the apical knob of receptor cells and their transient and steady state responses investigated with patch clamp techniques (Kleene and Gesteland, 1991a,b; Kleene, 1993; Kleene et al., 1994). This approach is ideal for the study of the olfactory transduction machinery.

Transduction

In olfactory cilia, odorant detection is initiated by heptahelical receptors, which induce a rise in the second messenger cAMP (Fig. 1). Subsequently, cyclic nucleotide-gated channels (cNg channels) open (Nakamura and Gold, 1987). Ca^{2+} and Na^+ ions then flow into the filamentous intraciliary space (Frings et al., 2000a). Ca^{2+}-activated chloride channels open and inward chloride current now contributes substantially to the receptor current (Kleene and Gesteland, 1991a; Kleene, 1993; Lowe and Gold, 1993; Schild and Restrepo, 1998; Frings et al., 2000b).

Na^+ ions are probably eliminated from the cilia by a Na^+-K^+ pump (Kern et al., 1991; Menco et al., 1998), usually a low-capacity device working in the background (e.g., Rasmusson et al., 1990). Ca^{2+} ions are eliminated from the cilia by a Na^+-Ca^{2+} exchanger of high capacity (Reisert and Matthews, 1998). Furthermore, a Ca^{2+} pump is likely to eliminate Ca^{2+} ions and thus contribute to the reconstitution of the resting state (Lo et al., 1994). A model of olfactory cilia, therefore, has to account

Received for publication 18 October 2000 and in final form 11 January 2001.

Address reprint requests to Bernd Lindemann, Dept. of Physiology, Universität des Saarlandes, D-66421 Homburg, Germany. Tel.: 49-6841-166464; Fax: 49-6841-166060; E-mail: phblin@med-rz.uni-sb.de.

0006-3495/01/04/1712/10 $2.00

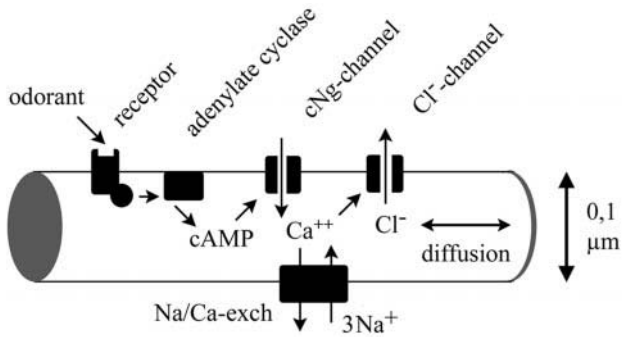

FIGURE 1 Scheme of principal transduction elements in olfactory cilia. The mean ciliary diameter is 0.1 μm in the rat and 0.2 μm in the frog. Not represented are the Na^+-K^+ pump and the Ca^{2+} pump.

for the activity of ion channels, a Ca^{2+} pump, a Na^+ pump, and a Na^+-Ca^{2+} exchanger in the plasma membrane and for ion diffusion gradients in the core of the cilium.

The modeled cNg conductance (Fig. 1) allowed simultaneous inflow of Ca^{2+} and Na^+ ions and outflow of K^+ ions. The Ca^{2+} fraction of this current (see Fig. 4 *C*) was typically set to >0.8 (Dzeja et al., 1999; Frings et al., 2000a). The Ca^{2+}-activated Cl^- conductance was modeled with a K_M value for Ca^{2+} of 4.8 μM and a Hill coefficient of 2 (Kleene and Gesteland, 1991a). A uniform distribution of channels was assumed to exist on the ciliary membrane (Lowe and Gold, 1991). Their fully activated conductances were scaled to yield total currents of 20 to 80 pA flowing through the basal cross-section of the cilium (e.g., Firestein and Werblin, 1989; Kleene and Gesteland, 1991b).

Concentrations and voltage

The base of the cilium was in contact with a comparatively large reservoir, representing the cytosol of olfactory knob, dendrite, and soma, or the quasi-intracellular solution facing the orifice of an excised cilium. The reservoir had constant chloride (80 mM), potassium (140 mM), sodium (4 mM), and calcium concentrations (30 nM). The most critical of these values, the chloride concentration, is based on recent measurements using a fluorescent dye (Kaneko et al., 2000). Other measurements, utilizing energy-dispersive X-ray microanalysis, yielded similar values, near 70 mM (Reuter et al., 1998). Throughout reservoir and cilium, a uniform concentration of immobile anions (64 mM) was assumed. The mucosal compartment, in contact with the ciliary surface, had constant chloride (55 mM), potassium (60 mM), sodium (60 mM), and calcium concentrations (3 mM).

The trans-ciliary voltage clamp potential (V_c) was set to -80 mV, reference being the uniform potential of the mucosal solution. Therefore, the electrical potential at any point along the ciliary axis was equal to the local membrane potential V_x, which was smaller than V_c whenever an axial potential profile developed. Since the cilium is thin, radial gradients of voltage and concentrations were considered negligible with respect to axial gradients.

Geometry and space for free diffusion

Olfactory cilia in the rat have diameters of 0.2 μm at the base and taper toward the tip. Their mean outside diameter is near 0.1 μm. With an effective membrane thickness of 3 nm, the mean inner diameter is 0.094 μm. The length is 20 to 30 μm in the rat, but 100 to 200 μm in the frog (Lidow and Menco, 1984). Thus, the ciliary volume of the rat will be 0.007 fL/μm length. This volume is in part occupied by a backbone of microtubules (9 + 2 pattern in proximal segments but merely 2 microtubules in medial and distal segments), leaving a free solution space or water-filled volume (WFV) that must be smaller than the ciliary volume. The WFV may be considered as an unstirred, filamentous continuum. Ions flowing into this volume through membrane channels will rapidly increase their local concentration. On the other hand, diffusion in the axial direction will equilibrate the WFV of different segments of a cilium with each other and with the bulk volume of the olfactory cell.

The volume fraction γ available for free diffusion is not known with precision but may be in the 30–60% range (see Lidow and Menco, 1984). Therefore, the WFV of the model cilium was chosen, somewhat arbitrarily, as 40% of the ciliary volume, i.e., 0.0028 fL/μm length. The segment length used for spatial discretization was $\Delta x \leq 1$ μm (see Appendix). The effective cross-sectional area available for diffusion was $A_D = 0.0028$ μm^2. For the WFV, diffusion coefficients for diffusion in water were used (e.g., Hille, 1992).

A constant radius r, that close to the base of the cilium, was used, ignoring the taper, thereby slightly underestimating concentration profiles. By varying r (Fig. 2), it was found that the general shape of profiles was robust and not critically dependent on particular values of r.

Transmembrane currents

For modeling, the cilium was treated as a cable of radius r and length L, delimited by a plasma membrane and filled with electrolyte. The radius being small, the membrane potential V and also the four internal ion concentrations c_k varied with position x on the cable axis, if current flowed across the membrane. Thus, five variables changed with location: the electrical potential V_x and the four concentrations $c_{Na,x}$, $c_{K,x}$, $c_{Ca,x}$ and $c_{Cl,x}$.

At the membrane, the current for ion species k depended on the local membrane potential and the local ion concentration. For this dependence the Goldman-Hodgkin-Katz (GHK) relationship was chosen for simplicity (Hille, 1992).

$$I_{k,x}^{chan} = P_k V_x (z_k F)^2 / RT \cdot \frac{c_{k,x} - c_{k,o}\xi_x}{1 - \xi_x} \quad [A/cm^2] \qquad (1)$$

in which $c_{k,o}$ is the constant concentration of species k in the outer medium, P_k the permeability and $\xi_x = \exp(-V_x z_k F/RT)$. R, T, z, and F have their usual meaning. Eq. 1 was used to model current through cNg channels and through Cl^- channels. When needed, alternatives for the GHK relationship can easily be substituted. Capacitive currents, of course, are absent in the steady state ($dV_x/dt = 0$).

Ca^{2+} activation of the chloride conductance was formulated according to Kleene and Gesteland (1991a) as

$$P_{Cl,x} = P_{Cl}^{max} \cdot \left(\frac{c_{Ca,x}}{c_{Ca,x} + K_{M,Ca}} \right)^H, \qquad (2)$$

in which H, the Hill coefficient, was set to 2, and 2 μM was used for $K_{M,Ca}$, yielding a $K_{1/2}$ of 4.8 μM.

The Ca^{2+} dependence of active Ca^{2+} transport (Rasmusson et al., 1990) may be described by

$$I_x^{Ca\text{-}pump} = I_{max}^{Ca\text{-}pump} \cdot \frac{c_{Ca,x}}{c_{Ca,x} + K_{M,p}}, \qquad (3)$$

where $I_x^{Ca\text{-}pump}$ is the outward current generated by the Ca^{2+} pump at location x. The effect of membrane voltage on the pump current is neglected in this relationship, restricting the use of Eq. 3 to moderate changes of V_x.

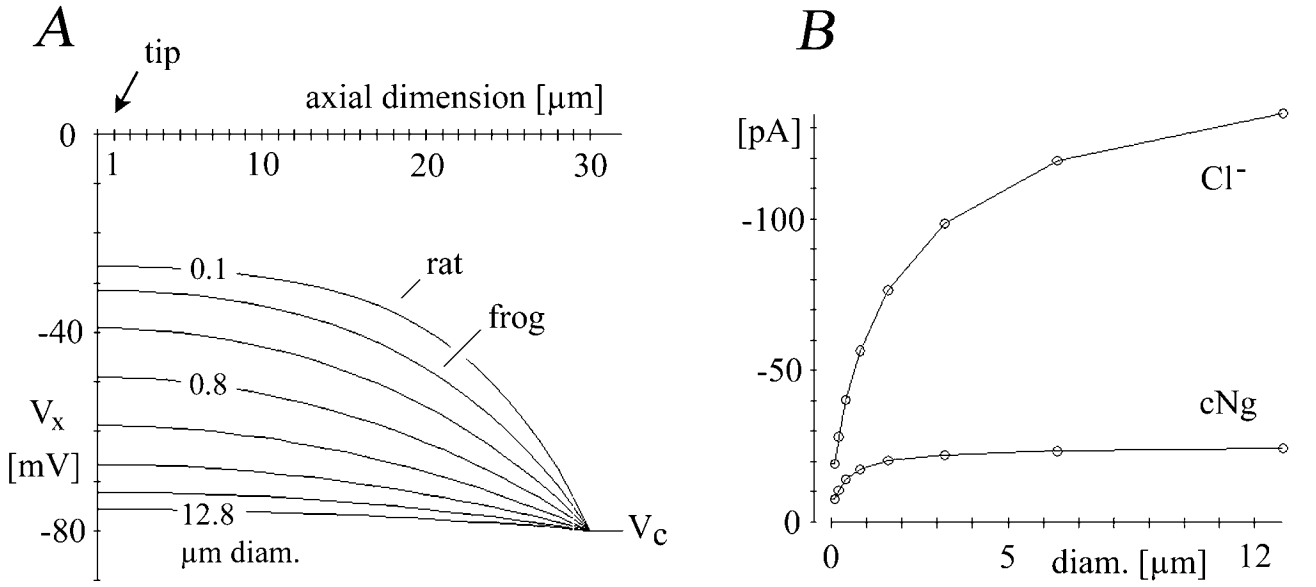

FIGURE 2 (*A*) The ciliary potential profile along the axial dimension (V(x)) during flow of transduction current. The tip of the cilium is on the left, the base on the right. Ciliary diameter was progressively doubled beginning with 0.1 μm, as indicated. The vertical distance between abscissa and curve represents the membrane potential V_j of a segment, and the vertical distance between curve and $V_c = -80$ mV represents the electrodiffusional potential between the segment and the base of the cilium. Note that the constant factors a_k and b_k in Eq. 6 contain the product $D_k\gamma r^2$. Therefore, the increase in r shown in the figure may be rescaled to an increase in either D_k or γ. Although, strictly speaking, a space constant is not defined for a cable with core electrodiffusion (see Appendix), the approximate electrotonic length was $\lambda \approx 8$ μm for the uppermost curve of this set. (*B*) Partial currents flowing through the basal cross-section as a function of ciliary diameter. The partial basal currents were computed by integrating partial membrane currents along the axial dimension. Cl^-, chloride current; cNg, current through cNg channels (essentially Ca^{2+} current). The dependence of currents on diameter shows that axial electrodiffusion was rate-limiting, especially at small diameters.

The outward current generated by the Na^+-K^+ pump (sodium pump) was modeled according to Rasmusson et al. (1990):

$$I_x^{\text{Na-pump}} = p_1 \cdot \left(\frac{c_{\text{Na,x}}}{c_{\text{Na,x}} + K_{\text{Na}}}\right)^3 \cdot \left(\frac{c_{\text{K,x}}}{c_{\text{K,x}} + K_{\text{K}}}\right)^2 \cdot \left(\frac{V_x + k_{\text{V1}}}{V_x + k_{\text{V2}}}\right) \tag{4}$$

in which p_1 is a scaling constant, $K_{\text{Na}} = 5.46$ mM, $K_{\text{K}} = 0.6$ mM, $k_{\text{V1}} = 150$ mV, and $k_{\text{V2}} = 200$ mV. The contributions of the pump current to Na^+ and K^+ transport were $I_{\text{Na,x}}^{\text{Na-pump}} = 3 \cdot I_x^{\text{Na-pump}}$ and $I_{\text{K,x}}^{\text{Na-pump}} = -2 \cdot I_x^{\text{Na-pump}}$.

The current carried by a Na^+-Ca^{2+} exchanger has a complex dependence on Na^+ and Ca^{2+} concentrations and membrane voltage (Mullins, 1977). At intermediate complexity (DiFrancesco and Noble, 1985) and for a Na^+/Ca^{2+} transport ratio r the relationship is given by

$$I_x^{\text{ex}} = k_1 \frac{(c_{\text{Na,x}}^r \cdot c_{\text{Ca,o}}/\xi_x) - (c_{\text{Na,o}}^r \cdot c_{\text{Ca,x}} \cdot \xi_x)}{1 + k_2 \cdot (c_{\text{Na,x}}^r \cdot c_{\text{Ca,o}} + c_{\text{Na,o}}^r \cdot c_{\text{Ca,x}})} \tag{5}$$

in which k_1 is a scaling constant and $\xi_x = \exp(-0.5\ V_x(r-2)F/RT)$. k_2 is an affinity constant which is, in first approximation, inversely related to the half-saturation value for $c_{\text{Ca,x}}$: $K_{0.5}^{\text{Ca}} = (k_2 \cdot c_{\text{Na,o}}^r)^{-1}$. With $r = 3$, the value of k_2 was chosen to give a half-saturation value of 4.6 μM, making the exchanger a high-threshold transporter. The contributions of the exchange current to Na^+ and Ca^{2+} transport were $I_{\text{Na,x}}^{\text{ex}} = 3 \cdot I_x^{\text{ex}}$ and $I_{\text{Ca,x}}^{\text{ex}} = -2 \cdot I_x^{\text{ex}}$.

The steady state electrodiffusional cable equation

Axial electrodiffusion in the steady state generates a one-dimensional, coaxial current $J_{\text{k,x}}$ for ion species k through the cable cross-section $A_D = \gamma r^2 \pi$, where γ defines the volume fraction available for the WFV. This current is for location x on the cable given by the Nernst Planck equation, a relationship which additively combines Fick's and Ohm's law:

$$J_{\text{k,x}} = a_k \frac{dc_{\text{k,x}}}{dx} + b_k c_{\text{k,x}} \frac{dV_x}{dx} \quad [\text{A}] \tag{6}$$

in which

$$a_k = z_k F \cdot D_k \cdot A_D \quad \left[\frac{\text{coul}}{\text{mole}} \cdot \frac{\text{cm}^4}{\text{s}}\right]$$

$$b_k = a_k \cdot z_k F/RT, \quad \left[\frac{\text{coul}}{\text{mole}} \cdot \frac{\text{cm}^4}{\text{s·mV}}\right]$$

where D_k is the diffusion coefficient in water and A_D the area available for diffusion. V_x and RT/F are conveniently expressed in mV. The signs in Eq. 6 account for the fact that outward membrane current and, therefore, axial current from base to tip are defined as positive, whereas x increases from tip to base.

In the steady state (each $dc_{\text{k,x}}/dt = 0$), not only the total current but also the partial currents are preserved by a continuity relationship for anyone location x:

$$\frac{dJ_{\text{k,x}}}{dx} = 2r\pi \cdot (I_{\text{k,x}}^{\text{chan}} + I_{\text{k,x}}^{\text{pump}} + I_{\text{k,x}}^{\text{ex}}) \quad \left[\frac{\text{A}}{\text{cm}}\right] \tag{7}$$

Therefore, differentiating Eq. 6 and combining it with the equations for membrane currents yields:

$$a_{Na}\frac{d^2c_{Na,x}}{dx^2} + b_{Na}\frac{dc_{Na,x}}{dx}\cdot\frac{dV_x}{dx} + b_{Na}c_{Na,x}\cdot\frac{d^2V_x}{dx^2} - 2r\pi\cdot(I^{chan}_{Na,x} + I^{ex}_{Na,x} + I^{Na\text{-}pump}_{Na,x}) = 0 \quad (7a)$$

$$a_{K}\frac{d^2c_{K,x}}{dx^2} + b_{K}\frac{dc_{K,x}}{dx}\cdot\frac{dV_x}{dx} + b_{K}c_{K,x}\cdot\frac{d^2V_x}{dx^2} - 2r\pi\cdot(I^{chan}_{K,x} + I^{Na\text{-}pump}_{K,x}) = 0 \quad (7b)$$

$$a_{Ca}\frac{d^2c_{Ca,x}}{dx^2} + b_{Ca}\frac{dc_{Ca,x}}{dx}\cdot\frac{dV_x}{dx} + b_{Ca}c_{Ca,x}\cdot\frac{d^2V_x}{dx^2} - 2r\pi\cdot(I^{chan}_{Ca,x} + I^{Ca\text{-}pump}_{Ca,x} + I^{ex}_{Ca,x}) = 0 \quad (7c)$$

$$a_{Cl}\frac{d^2c_{Cl,x}}{dx^2} + b_{Cl}\frac{dc_{Cl,x}}{dx}\cdot\frac{dV_x}{dx} + b_{Cl}c_{Cl,x}\cdot\frac{d^2V_x}{dx^2} - 2r\pi\cdot(I^{chan}_{Cl,x}) = 0 \quad (7d)$$

We have thus obtained a set of four ordinary, nonlinear, second order differential equations, which represent the steady state cable formalism for the case of ion concentration gradients within the cable. In addition, the condition for bulk electroneutrality (Finkelstein and Mauro, 1977) is to be included:

$$c_{Na,x} + c_{K,x} + 2c_{Ca,x} - c_{Cl,x} - c_A = 0, \quad (7e)$$

in which c_A (concentration of immobile anions) is a constant. With Eq. 7e, we have five equations and five unknowns.

The boundary conditions for a cable of length L, closed at the tip ($x = 0$) but open at the base, are

$$\text{At } x = 0 \quad \frac{dV_x}{dx} = 0 \quad \frac{dc_{k,x}}{dx} = 0$$

$$\text{At } x = L \quad V_L = V_c \quad c_{k,L} = c_{k,c},$$

in which V_c and $c_{k,c}$ are constants.

The relationship between the electrodiffusional cable formalism (Eq. 7) and the classical cable equation is discussed in the Appendix. Segmentation, discretization strategies, and numerical procedures are also detailed in the Appendix.

RESULTS

Voltage profile

With transduction currents switched on, membrane voltage varied considerably along the ciliary axis, as shown in Fig. 2 *A*. The V_x profile was steeper toward the base of the cilium, where the axial current became larger (see below), as expected for a leaky cable closed at one end and open at the other. However, unlike that of a classical cable, the voltage profile contained axial diffusion potentials associated with concentration gradients. Their values were calculated by adding the Nernst-Planck equation (the discretized form of Eq. 6 was used) for all ion species k, setting for a given x the sum of $J_{k,x}$ to zero and solving for ΔV_x. The result $\Delta V_x^{J=0}$ was the instantaneous value of the local axial potential, observed when all membrane transport was suddenly halted, causing the net axial current to vanish.

When using 30 segments, $\Delta V_x^{J=0}$ was usually less than 1 mV per segment (Figs. 3 *D* and 4 *D*). It should be noted that the diffusion gradients in the cilium are mainly those of K^+ and Cl^-, ions of similar diffusion coefficients. This explains the comparatively small values of $\Delta V_x^{J=0}$ in this special situation. $\Delta V_x^{J=0}$ changed sign when followed along the axis (Figs. 3 *D* and 4 *D*). This was due to the additional diffusion gradients of Ca^{2+} ions in proximal segments (see below).

The profiles of membrane voltage for the ciliary diameters of 0.1 and 0.2 μm (Fig. 2 *A*) show that the space clamp must be quite poor in voltage clamp experiments with excised cilia of rat and frog (see also Larsson et al., 1997). When the ciliary diameter was increased, keeping the value of the membrane conductances constant, the V_x profiles flattened. At the same time, the currents flowing through the base of the cilium increased (Fig. 2 *B*). The increase was due to the change in membrane voltage and ciliary ion concentrations, which resulted from the enlargement of the diffusional cross-section. It showed that most of the ciliary ion transport was limited by axial electrodiffusion.

Concentration profiles

Consequences of chloride outflow

It is a basic feature of ciliary ion transport that Ca^{2+}-activated, anion-conducting channels allow flow of inward current. As this current direction means outward movement of Cl^- ions, depletion of Cl^- ions had to occur in the model cilium. The ion depletion was only partially compensated by coaxial, electrodiffusional resupply of chloride ions from the base of the cilium and was strongest at the tip and in distal segments, where diffusional replenishment was more difficult (Figs. 3 *A* and 4 *A*). A parallel depletion of K^+ ions occurred in addition, driven by the requirement for electroneutrality. The membrane current carried by Cl^- ions was not uniform but, due to the profile of Cl^- concentration, maximal in proximal segments (Figs. 3 *C* and 4 *C*). Yet, as the cilium was voltage clamped to $V_c = -80$ mV, the driving force for movement of chloride ions continued to be outward even in distal segments (driving inward current), despite the changes in the local membrane potential V_x and Nernst potential $E_{Cl,x}$.

Ca^{2+} inflow, Ca^{2+} flooding

In the absence of Ca^{2+} export, the ciliary Ca^{2+} concentration rose to millimolar values. This was a consequence of the fact that Ca^{2+} was the major carrier of current in the cNg-channels and that this current was directed into the small WFV of the cilia. A rough calculation may serve to illustrate this. When the cNg channels open at the onset of

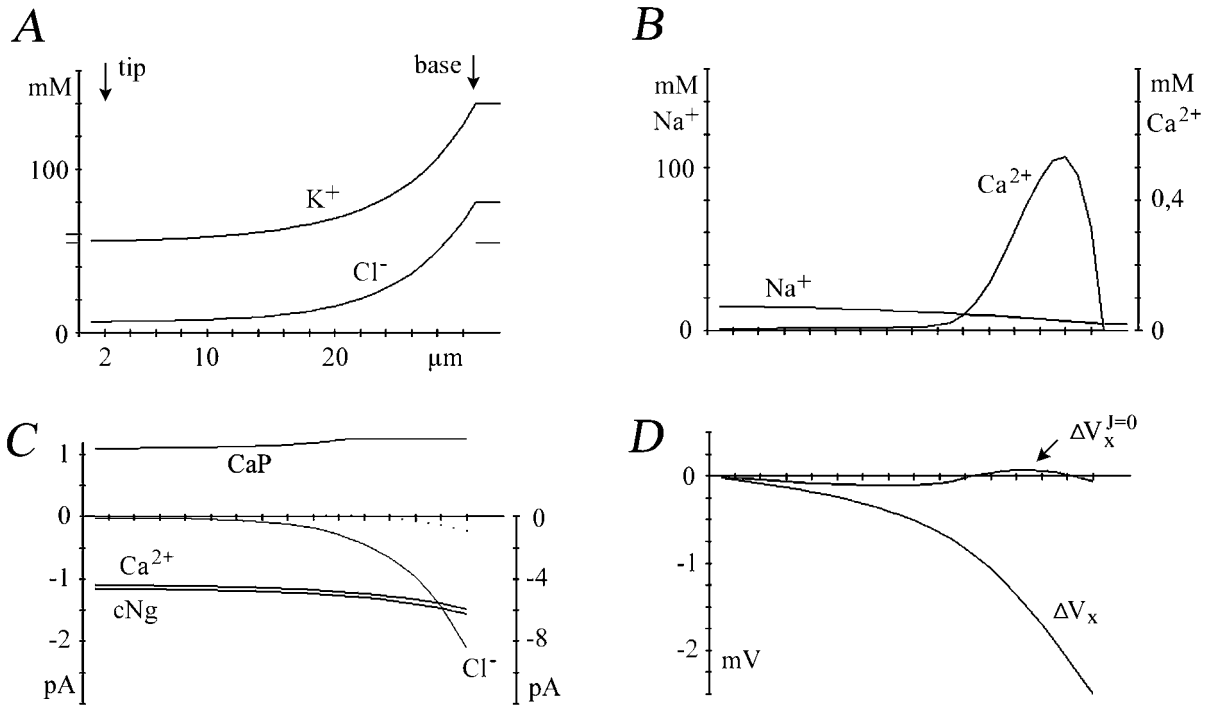

FIGURE 3 Axial profiles of concentrations, currents and voltages. In this simulation, Ca^{2+} extrusion was exclusively due to the Ca^{2+} pump. The ciliary diameter was 0.2 μm. (*A*) Profiles of Cl^- and K^+ concentrations. The depletion of both ions in distal segments is obvious. (*B*) Profiles of Na^+ and Ca^{2+} concentrations. In the distal segments, the Ca^{2+} concentration was lower than 7 μM. (*C*) Profiles of membrane currents through chloride channels (labeled Cl^-, scale on the right) and cyclic nucleotide-gated channels (cNg). The Ca^{2+} component of the cNg-current is labeled Ca^{2+}. The outward current through the Ca^{2+}-pump is shown above (CaP). (*D*) Voltage profiles. ΔV_x is the change of the electrodiffusional voltage per segment, $\Delta V_x^{J=0}$ its non-ohmic component. Currents leaving the cilium through the basal cross-section were as follows (in pA): cNg, −37.8; Ca^{2+} component, −35.8; Ca^{2+} pump, 35.1; Cl^- current, −47.5.

transduction and pass the inward current i_{Ca}^{chan}[A], the initial change of c_{Ca} with time is given by

$$\frac{dc_{Ca}}{dt} = \frac{-i_{Ca}^{chan}}{2F \cdot \mathrm{WFV}} \tag{8}$$

This amounts to 60 mM/s/pA, suggesting a rapid rise to high values. The more detailed steady state calculation is provided by the numerical simulations. The Ca^{2+} flooding of the WFV demonstrated the necessity for Ca^{2+} export through the ciliary membrane, since diffusion in the axial dimension obviously did not suffice to keep the c_{Ca} low, and buffering cannot cope with these large amounts of Ca^{2+} ions. Moreover, it was impossible to include Ca^{2+} buffers because their contribution cancelled out in the steady state ciliary system.

Ca^{2+} export

By activating the Ca^{2+} pump, the ciliary Ca^{2+} concentration could be lowered. However, despite a uniform distribution of channels and pumps, the resulting Ca^{2+} profile was not uniform: in proximal segments a pronounced Ca^{2+} peak was found (Fig. 3 *B*). It was due to the fact that the Ca^{2+} inward current changed with voltage (Eq. 1). This current was, therefore, stronger in proximal segments, whereas current through the Ca^{2+} pump (Eq. 3) changed much less across segments. These two currents are compared in Fig. 3 *C*. The voltage effects described here are effects of driving force and are not due to voltage-gating.

Active Ca^{2+} transport is usually a background mechanism of high affinity and low capacity (DiPolo and Beaugé, 1983). It is unlikely that this mechanism carries the main load of rapid Ca^{2+} export in the cilia, especially since it would not explain that a decrease in mucosal Na^+ concentration causes prolongation of the transduction current. This observation has suggested a Na^+-dependent Ca^{2+} extrusion by means of Na^+-Ca^{2+} exchange (Reisert and Matthews, 1998).

Implementation of a Na^+-Ca^{2+} exchanger into the model showed that this device was unable to decrease the ciliary Ca^{2+} concentration to values below 6 mM. The reason was the increase in ciliary Na^+ concentration effected by the exchange, removing the Na^+ gradient required for outward movement of Ca^{2+} ions. Therefore, a Na^+-K^+ pump was implemented parallel to the Na^+-Ca^{2+} exchanger. This device kept the ciliary Na^+ concentration small and allowed

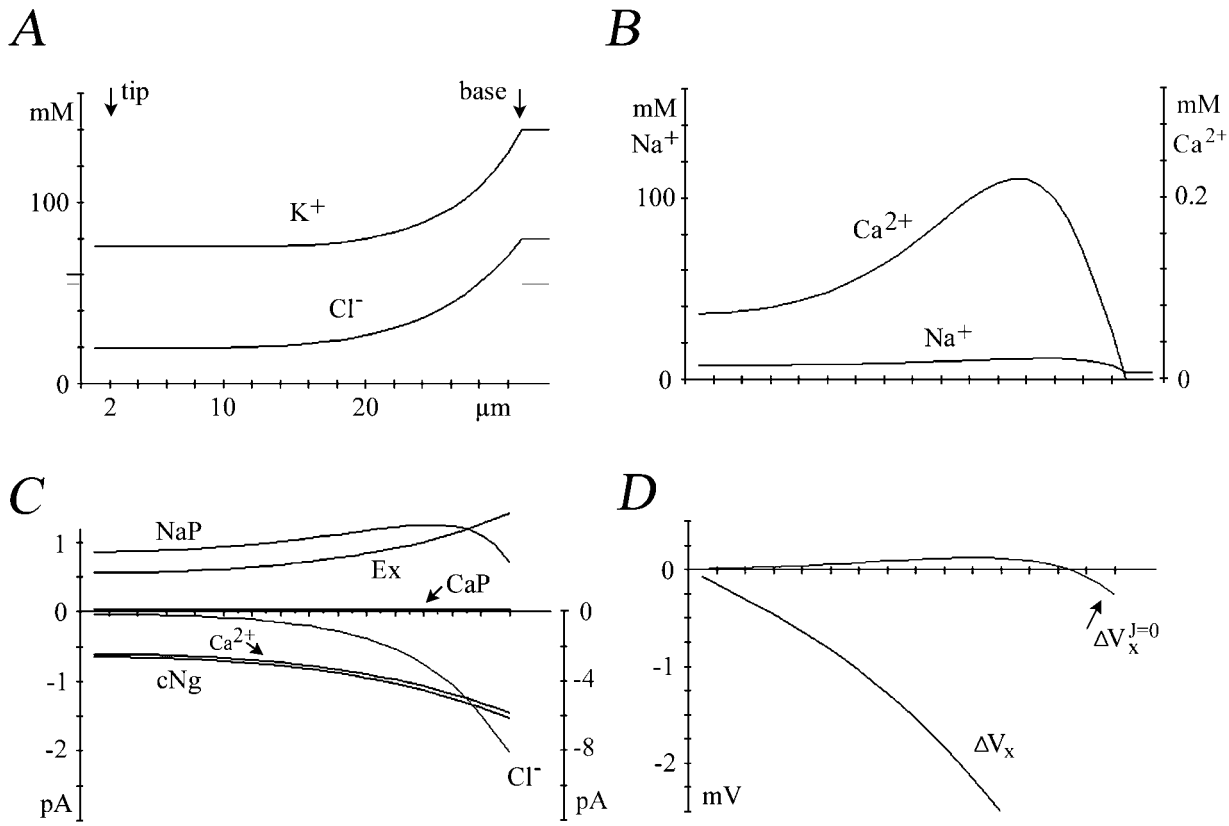

FIGURE 4 Axial profiles of concentrations, currents, and voltages. In this simulation, Ca^{2+} extrusion was mainly due to the Na^+-Ca^{2+} exchanger, which was paralleled by a Na^+-K^+ pump. The ciliary diameter was 0.2 μm. (*A*) Profiles of Cl^- and K^+ concentrations. Note that the distal K^+ concentration was higher than in Fig. 3 *A* by 20 mM, due to the action of the Na^+-K^+ pump. The Cl^- concentration was also higher for reasons of electroneutrality. (*B*) Profiles of Na^+ and Ca^{2+} concentrations. Note that the proximal Ca^{2+} peak was less steep than in Fig. 3 *B*, due to the voltage dependence of the Na^+-Ca^{2+} exchange. (*C*) Profiles of membrane currents through chloride channels (labeled Cl^-, scale on the right), cyclic nucleotide-gated channels (cNg) and the Na^+-Ca^{2+} exchanger (Ex). The Ca^{2+} component of the exchange is shown, to ease comparison with the Ca^{2+} component of the cNg current (labeled Ca^{2+}). NaP, Na^+-K^+ pump; CaP, Ca^{2+} pump. (*D*) Voltage profiles. ΔV_x is the change of the electrodiffusional voltage per segment, $\Delta V_x^{J=0}$ its non-ohmic component. Currents leaving the cilium through the basal cross-section were as follows (in pA): cNg, −27.2; Ca^{2+} component, −25.7; Na^+-Ca^{2+} exchanger, −12.1; Ca^{2+} component, 24.2; Na^+-K^+ pump 10.3; Ca^{2+} pump, 1.4; Cl^- current, −53.6.

the exchanger to decrease the ciliary Ca^{2+} concentration to values below 100 μM in distal segments (Fig. 4 *B*). In proximal segments, however, the axial Ca^{2+} profile retained a peak, which was due to a difference in the voltage dependence of import and export processes, as shown in Fig. 4 *C*.

DISCUSSION

Significance of steady state modeling

Olfactory cilia have been extensively investigated in the steady state. Furthermore, even the transient responses, recorded after application of olfactory stimuli, have long durations on the order of seconds, suggesting that steady state conditions might be approached. Therefore, the modeling of ciliary ion dynamics in the steady state is of interest. Moreover, it provides the foundation for future modeling of transient responses.

Voltage profile

The voltage profile, which had the general shape expected from a leaky cable with only one open end, was pronounced with ciliary diameters of 0.1 μm (rat) or 0.2 μm (frog) and transduction currents on the order of 50 pA. Therefore, the space clamp must be quite poor in voltage clamp experiments with excised cilia of rat and frog, as previously noted by Larsson et al. (1997).

Chloride currents

Due to outward flow of chloride ions, these ions were depleted especially in distal segments, where diffusional resupply from the base was most difficult. For reasons of electroneutrality, this change was accompanied by a depletion of K^+ ions. The K^+ ions were lost by diffusion in the axial direction. In consequence of the Cl^- depletion, the

chloride current through the ciliary membrane was not uniform but increased towards the base of the cilium. The maximum was found in those proximal segments where the ciliary Cl^- concentration driving this current was high enough and the Ca^{2+} concentration activating this current was also high enough. The Cl^- depletion is likely to codetermine the time course of the receptor potential or current.

The present model used five transport elements, all of which are known to occur in olfactory cilia. Other, undiscovered elements may also contribute. For instance, a strong cation-chloride cotransport, as known from other neurons (Ehrlich et al., 1999), might serve for Cl^- accumulation and thus limit the development of Cl^- profiles. However, there is presently no experimental basis for inclusion of this transporter into a ciliary model. Of foremost interest, therefore, is the future measurement of ciliary chloride concentrations, both in the resting state and during stimulation.

Ca^{2+} profile

Due to the small ciliary volume and the large Ca^{2+} fraction of the transduction current, the steady state Ca^{2+} concentration exceeded 20 millimolar when the membrane transport of Ca^{2+} ions was limited to channels and V_c clamped to -80 mV. To check this Ca^{2+} flooding, the steady state model used transporters like the Na^+-Ca^{2+} exchanger to provide for Ca^{2+} export.

The axial voltage profile affected Ca^{2+} inflow and Ca^{2+} export differently. The Ca^{2+} inflow through cNg channels varied strongly with membrane voltage, the ionic charge moved being $+2$ per ion. Therefore, the inflow followed the V_x profile: small in distal segments but rising toward the base of the cilium. In contrast, the voltage effect on Ca^{2+} export through the Na^+-Ca^{2+} exchanger was smaller. With a Na^+/Ca^{2+} coupling ratio of 3, the charge governing this dependence was $+1$. Export through the Na^+-Ca^{2+} exchanger was, in addition, affected by the Na^+ profile. The result was an outward current that increased toward the base of the cilium, but slightly less than the Ca^{2+} inward current mediated by channels.

In consequence, Ca^{2+} inflow exceeded export at all locations, the difference being maximal in proximal segments. In conjunction with Ca^{2+} diffusion towards the base, these relationships caused a Ca^{2+} profile having a maximum in proximal segments. The two determinants of the Ca^{2+} accumulation in proximal segments, an axial voltage profile and a difference in voltage dependence between Ca^{2+} import and export processes, probably are common constellations in the leaky cables associated with neurons.

The Na^+-Ca^{2+} exchanger can eliminate ciliary Ca^{2+} only by increasing ciliary Na^+. It turned out that the increasing Na^+ concentration stopped the elimination process such that values below 6 mM of ciliary Ca^{2+} concentration could not be attained. However, this limit was substantially lowered when the Na^+-K^+ pump was incorporated into the model. The pump kept the ciliary Na^+ concentration low and permitted the exchanger to decrease the ciliary Ca^{2+} concentration to <100 μM in distal segments. In proximal segments, however, larger Ca^{2+} concentrations persisted for the reasons detailed above. These observations suggest that the Na^+-Ca^{2+} exchange is accompanied by active Na^+ transport of comparable capacity in the ciliary membrane. A sodium pump located in the membranes of knob and dendrite is not sufficient. The presence of a sodium pump on the cilia was previously indicated by immunohistochemistry (Kern et al., 1991; Menco et al., 1998).

It is interesting that recent measurements of the ciliary Ca^{2+} concentration with fluorescence techniques consistently showed low values, below 300 nM, during transduction (Leinders-Zufall et al., 1997, 1998b,a). These low concentrations, which are not sufficient to activate the Ca^{2+}-dependent Cl^- currents (Kleene and Gesteland, 1991a), are rather unexpected in view of the strong Ca^{2+} inward currents mediated by the cNg channels (Dzeja et al., 1999; Frings et al., 2000a). Which mechanisms may limit the expected Ca^{2+} flooding?

Escape toward the dendrite by axial electrodiffusion does contribute. However, according to the present simulations this process is not rapid enough to keep the Ca^{2+} concentration low.

Uptake by vesicular Ca^{2+} stores is unlikely, because membrane-bound compartments are seldom found or absent within the cilia (Arstila and Wersäll, 1967; Menco, 1984; Lidow and Menco, 1984; Menco, 1997) and Ca^{2+} release from intraciliary stores could not be demonstrated (Leinders-Zufall et al., 1998b; Zufall et al., 2000).

Ca^{2+} binding proteins, like calmodulin (e.g., Chen and Yau, 1994; Kleene, 1994), are present in the cilia and will act as buffers. However, protein-Ca^{2+} buffers with concentrations in the lower mM range will hardly cope with an increase in Ca^{2+} concentration of 60 mM/s/pA (Eq. 8).

Export by a Ca^{2+} pump and by the Na^+-Ca^{2+} exchanger may limit the expected Ca^{2+} flooding. The pump is usually a low-capacity background device which cannot eliminate Ca^{2+} rapidly (DiPolo and Beaugé, 1983; Rasmusson et al., 1990). In contrast, the exchanger appears to be of high capacity (Reisert and Matthews, 1998). Most likely, a high-capacity Na^+-Ca^{2+} exchanger, serving for Ca^{2+} export during recovery, may also have a role in the transduction phase preceding recovery. However, as shown above, the exchanger must be accompanied by a sodium pump.

Distribution of transport elements

The transport elements were distributed uniformly in the model. Although this seemed justified by electrophysiology (Lowe and Gold, 1991), morphological considerations and localization of G-protein and adenylate cyclase suggested that transduction occurs mainly in distal segments, which are closer to the air/mucus interface (Menco et al., 1992;

Menco, 1994). Moreover, immunohistochemistry has shown one subunit of the cNg channel labeled more strongly in distal segments (Matsuzaki et al., 1999). This emphasis on distal segments, however, might aggravate rather than relieve the diffusion limitation.

Ca^{2+} measurements with a fluorescent dye indicated uniform changes along the ciliary axis in response to 8-Br-cGMP, blockers of cyclic nucleotide breakdown (IBMX), or the cNg channel blocker (LY83583), all agents that act downstream of receptors (Leinders-Zufall et al., 1997). However, upon stimulating with odorants a more granular axial distribution (hot spots) was seen, which may be due to a heterogeneous distribution of receptors (Leinders-Zufall et al., 1998a). A nonuniform distribution of dye or cNg channels seems less likely in view of the earlier results with 8-Br-cGMP. A clustering of transduction elements in hot spots will not, of course, resolve the overall diffusion limitation of ciliary transport.

Conclusions

In summary, the ion transport system of olfactory cilia was successfully modeled as an electrodiffusional cable. In simulations using this formalism, the ciliary geometry had large effects on ion distributions and transduction currents. A consistent feature found was the Cl^- and K^+ depletion in distal segments. Because realistic values had been used for ciliary length and diameter, the depletion shows that ciliary ion transport is limited by axial electrodiffusion. However, the simulations included only those ion transporters that are known to exist on the cilia. Additional, unidentified transporters might also be present, possibly counteracting the development of large concentration changes within the cilia.

APPENDIX

Relationship to classical cable equation

A space constant is not defined for a cable with core electrodiffusion (Eq. 7, a–e), but can be derived for the limiting case of constant concentrations (each $dc_k/dx = 0$). To show this without difficulty, we shall for the membrane currents adopt a linear current voltage relationship:

$$I_{k,x} = g_k \cdot (V_x - E_k) \quad [A/cm^2] \tag{A1}$$

in which g_k is the conductance V/cm^2 and

$$E_k = \frac{RT}{z_k F} \cdot \ln\left(\frac{c_{k,o}}{c_k}\right) \quad [mV] \tag{A2}$$

the reversal potential, which does not change with location since concentrations are constant. By adding Eqs. 7a–d, one then obtains

$$\frac{d^2V_x}{dx^2} = 2r\pi \cdot \frac{\sum_k (g_k \cdot (V_x - E_k))}{\sum_k (b_k \cdot c_k)}.$$

Since the reversal potential V_r of the membrane is a weighted mean of all Nernst potentials E_k:

$$\sum_k (g_k \cdot E_k) = V_r \sum_k g_k,$$

one finds by insertion

$$\frac{d^2V_x}{dx^2} = \frac{V_x - V_r}{\lambda^2}, \tag{A3}$$

in which the space constant λ is given by

$$(\lambda)^2 = \frac{\sum_k b_k c_k}{2r\pi \cdot \sum_k g_k}. \quad [cm^2] \tag{A3a}$$

Eq. A3 is equivalent to the classical steady state cable equation (Rall, 1977), but modified to account for the effect of a reversal potential and by using the Ohmic term of the Nernst-Planck equation to describe coaxial current flow. The general solution is

$$V_x = A_1 \exp(x/\lambda) + A_2 \exp(-x/\lambda) \tag{A3b}$$

With the boundary conditions for a sealed end of the cable at $x = 0$ ($dV_0/dx = 0$) and an open and voltage-clamped end at $x = L$($V_L = V_c$), we arrive at

$$V_x = (V_c - V_r) \cdot \frac{\exp(x/\lambda) + \exp(-x/\lambda)}{\exp(L/\lambda) + \exp(-L/\lambda)} + V_r \tag{A3c}$$

Discretization and numerical procedures

To obtain numerical solutions for the boundary value problem of Eq. 7, we perform discretization in space by dividing the cable into n segments (index j). The segment length Δx must be much smaller than the space constant λ, which is given approximately by Eq. A3a. Values of $\Delta x \leq 1$ μm were used. Substitution with

$$\frac{d^2V_x}{dx^2} = \frac{1}{\Delta x^2} \cdot (V_{j+1} - 2 \cdot V_j + V_{j-1}),$$

$$\frac{dV_x}{dx} = \frac{1}{2\Delta x} \cdot (V_{j+1} - V_{j-1}), \quad V_x = V_j,$$

$$\frac{d^2c_{k,x}}{dx^2} = \frac{1}{\Delta x^2} \cdot (c_{k,j+1} - 2 \cdot c_{k,j} + c_{k,j-1}),$$

$$\frac{dc_{k,x}}{dx} = \frac{1}{2\Delta x} \cdot (c_{k,j+1} - c_{k,j-1}), \quad c_{k,x} = c_{k,j},$$

yields for ion species k

$$\frac{a_k}{\Delta x^2} \cdot (c_{k,j+1} - 2 \cdot c_{k,j} + c_{k,j-1}) + \frac{b_k}{4\Delta x^2} \cdot (c_{k,j+1} - c_{k,j-1}) \cdot (V_{j+1} - V_{j-1}) + \frac{b_k \cdot c_{k,j}}{\Delta x^2} \cdot (V_{j+1} - 2 \cdot V_j + V_{j-1}) - 2r\pi \cdot (I_{k,j}^{chan} + I_{k,j}^{pump} + I_{k,j}^{ex}) = 0. \tag{A4}$$

Corresponding equations were formulated for Na^+, K^+, Ca^{2+}, and Cl^-. For $j = 1$ and $j = n$ the appropriate boundary values were inserted. For $I_{k,j}^{chan}(V_j)$ current-voltage relationships other than the GHK relationship may be substituted. Furthermore, the sum of membrane currents may be supplemented by suitable expressions for currents through yet other membrane transporters.

The set of $5n$ algebraic, nonlinear equations (Eq. A4 applied to Na^+, K^+, Ca^{2+}, and Cl^-, plus Eq. 7e) had to be solved for the $5n$ unknowns, i.e., V_j and the concentrations $c_{Na,j}$, $c_{K,j}$, $c_{Ca,j}$, and $c_{Cl,j}$. Solutions were obtained iteratively with the Newton-Raphson procedure (Press et al., 1990; Sprott, 1991). Fig. 5 gives a graphical representation of the Jacobian matrix used.

The software written for this application was structured in modules, such that solutions could be obtained for axial electrodiffusion only and for combinations of electrodiffusion with ion transport through channels, Ca^{2+} pumping, Na^+-K^+ pumping, and Na^+-Ca^{2+} exchange. Furthermore, the Ca^{2+} activation of the Cl^- conductance could be enabled and/or disabled. The modular design proved helpful when stability problems arose (see below).

The Newton-Raphson procedure worked efficiently as long as axial electrodiffusion was combined with transport through channels only. In this case the number of iterations required was less than ten. However, when Ca^{2+} pump and/or Na^+-Ca^{2+} exchanger were added, many more iterations were needed, and often a solution could not be obtained. This was expected because the procedure is very sensitive to the initial values supplied, especially when highly nonlinear kinetics, like those for the Na^+-Ca^{2+} exchanger, are involved.

A way around this problem was to obtain a solution with one critical parameter, for instance the scaling constant k_1 of the exchanger (Eq. 5), set to a low value. This solution was then used as the initial condition of the next run, for which the critical parameter was slightly increased. Variable step size strategies were implemented to avoid steps too large or too small. Thereby, step size was adjusted such that a run took two iterations only. This strategy of migrating initial conditions proved tenable, even though in some cases a series of many runs was required to obtain a solution showing low Ca^{2+} concentrations in the cilium.

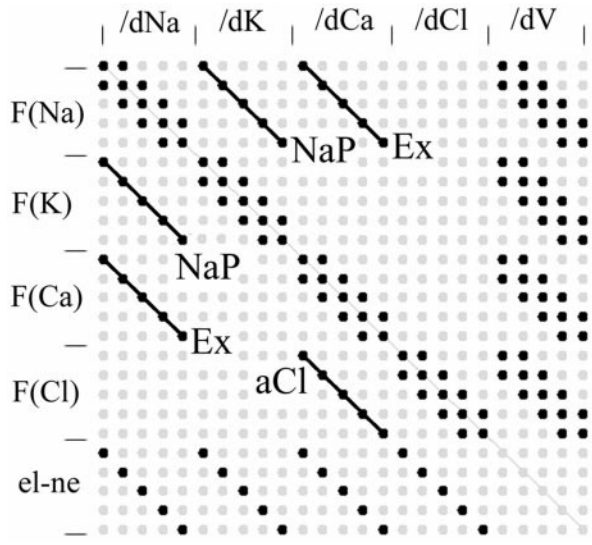

FIGURE 5 Structure of the Jacobian matrix used with the Newton-Raphson procedure. The matrix contains the derivatives of the functions F (Eq. 7 or A4) with respect (separately) to all variables, as shown. "el-ne" designates the representation of the electroneutrality condition (see Eq. 7e). Matrix elements of values $\neq 0$ are represented in black, the others in grey. For clarity, the number of segments was lowered from 30 to 5 for this plot. Ex, Na^+-Ca^{2+} exchanger (Eq. 5); NaP, Na^+-K^+ pump (Eq. 4); aCl, Ca^{2+}-activation of Cl^- current (Eq. 2).

Solutions were obtained in terms of axial profiles of voltage and concentrations. Based on these, membrane currents and axial currents were computed using the appropriate flow-driving force relationships. Partial currents through the base of the cilium were obtained by integrating the corresponding membrane currents along the axial dimension.

It is a pleasure to thank Dr. Bert Ph. M. Menco, Department of Neurobiology and Physiology, Northwestern University, for a discussion on ciliary morphology, Dr. Steven J. Kleene, Department of Cell Biology, Neurobiology and Anatomy, University of Cincinnati, for a discussion on the model parameters, and Herrn Volker Gebhard, Institut für Angewandte Mathematik, Universität des Saarlandes and Dr. Gregory D. Smith, Department of Mathematics, Arizona State University, for valuable advice on numerical strategies.

Supported by the Deutsche Forschungsgemeinschaft, SFB530/B2.

REFERENCES

Arstila, A., and J. Wersäll. 1967. The ultrastructure of the olfactory epithelium of the guinea pig. *Acta Oto-Laryngologica.* 64:187–204.

Chen, T. Y., and K. W. Yau. 1994. Direct modulation by Ca^{2+}-calmodulin of cyclic nucleotide-activated channel of rat olfactory receptor neurons. *Nature.* 368:545–548.

DiFrancesco, D., and D. Noble. 1985. A model of cardiac electrical activity incorporating ionic pumps and concentration changes. *Philos. Trans. R. Soc. Lond. B Biol. Sci.* 307:353–398.

DiPolo, R., and L. Beaugé. 1983. The calcium pump and sodium-calcium exchange in squid axons. *Annu. Rev. Physiol.* 45:313–324.

Dzeja, C., V. Hagen, U. B. Kaupp, and S. Frings. 1999. Ca^{2+} permeation in cyclic nucleotide-gated channels. *EMBO J.* 18:131–144.

Ehrlich, I., S. Lohrke, and E. Friauf. 1999. Shift from depolarizing to hyperpolarizing glycine action in rat auditory neurones is due to age-dependent Cl^- regulation. *J. Physiol. (Lond.).* 520 Pt 1:121–137.

Finkelstein, A., and A. Mauro. 1977. Physical principles and formalisms of electrical excitability. *In* Handbook of Physiology, Section 1: The Nervous System. E. R. Kandel, editor. Oxford University Press, New York. 161–213.

Firestein, S., and F. Werblin. 1989. Odor-induced membrane currents in vertebrate-olfactory receptor neurons. *Science.* 244:79–82.

Frings, S., D. H. Hackos, C. Dzeja, T. Ohyama, V. Hagen, U. B. Kaupp, and J. I. Korenbrot. 2000a. Determination of fractional calcium ion current in cyclic nucleotide-gated channels. *Methods Enzymol.* 315: 797–817.

Frings, S., D. Reuter, and S. J. Kleene. 2000b. Neuronal Ca^{2+}-activated Cl^- channels: homing in on an elusive channel species. *Prog. Neurobiol.* 60:247–289.

Hille, B. 1992. Ionic Channels in Excitable Membranes. Sinauer Associates Inc., Sunderland, MA.

Kaissling, K.-E. 1971. Insect olfaction. *In* Handbook of Sensory Physiology. L. M. Beidler, editor. Springer-Verlag, Berlin. 351–431.

Kaneko, H., T. Nakamura, and B. Lindemann. 2001. Non-invasive measurement of the chloride concentration in rat olfactory receptor cells, using a fluorescent dye. *Am. J. Physiol.* 280. in press.

Kern, R. C., T. P. Kerr, and T. V. Getchell. 1991. Ultrastructural localization of Na^+/K^+-ATPase in rodent olfactory epithelium. *Brain Res.* 546:8–17.

Kleene, S. J. 1993. Origin of the chloride current in olfactory transduction. *Neuron.* 11:123–132.

Kleene, S. J. 1994. Inhibition of olfactory cyclic nucleotide-activated current by calmodulin antagonists. *Br. J. Pharmacol.* 111:469–472.

Kleene, S. J., and R. C. Gesteland. 1991a. Calcium-activated chloride conductance in frog olfactory cilia. *J. Neurosci.* 11:3624–3629.

Kleene, S. J., and R. C. Gesteland. 1991b. Transmembrane currents in frog olfactory cilia. *J. Membr. Biol.* 120:75–81.

Kleene, S. J., R. C. Gesteland, and S. H. Bryant. 1994. An electrophysiological survey of frog olfactory cilia. *J. Exp. Biol.* 195:307–328.

Larsson, H. P., S. J. Kleene, and H. Lecar. 1997. Noise analysis of ion channels in non-space-clamped cables: estimates of channel parameters in olfactory cilia. *Biophys. J.* 72:1193–1203.

Leinders-Zufall, T., C. A. Greer, G. M. Shepherd, and F. Zufall. 1998a. Imaging odor-induced calcium transients in single olfactory cilia: specificity of activation and role in transduction. *J. Neurosci.* 18:5630–5639.

Leinders-Zufall, T., C. A. Greer, G. M. Shepherd, and F. Zufall. 1998b. Visualizing odor detection in olfactory cilia by calcium imaging. *Ann. N. Y. Acad. Sci.* 855:205–207.

Leinders-Zufall, T., M. N. Rand, G. M. Shepherd, C. A. Greer, and F. Zufall. 1997. Calcium entry through cyclic nucleotide-gated channels in individual cilia of olfactory receptor cells: spatio-temporal dynamics. *J. Neurosci.* 17:4136–4148.

Lidow, M. S., and B. P. Menco. 1984. Observations on axonemes and membranes of olfactory and respiratory cilia in frogs and rats using tannic acid-supplemented fixation and photographic rotation. *J. Ultrastruct. Res.* 86:18–30.

Lo, Y. H., T. M. Bradley, and D. E. Rhoads. 1994. High-affinity Ca^{2+}, Mg^{2+}-ATPase in plasma membrane-rich preparations from olfactory epithelium of Atlantic salmon. *Biochim. Biophys. Acta.* 1192:153–158.

Lowe, G., and G. H. Gold. 1991. The spatial distributions of odorant sensitivity and odorant-induced currents in salamander olfactory receptor cells. *J. Physiol. (Lond.).* 442:147–168.

Lowe, G., and G. H. Gold. 1993. Nonlinear amplification by calcium-dependent chloride channels in olfactory receptor cells. *Nature.* 366: 283–286.

Lumpkin, E. A., and A. J. Hudspeth. 1998. Regulation of free Ca^{2+} concentration in hair-cell stereocilia. *J. Neurosci.* 18:6300–6318.

Matsuzaki, O., R. E. Bakin, X. Cai, B. P. Menco, and G. V. Ronnett. 1999. Localization of the olfactory cyclic nucleotide-gated channel subunit 1 in normal, embryonic and regenerating olfactory epithelium. *Neuroscience.* 94:131–140.

Menco, B. P. 1984. Ciliated and microvillous structures of rat olfactory and nasal respiratory epithelia. A study using ultra-rapid cryo-fixation followed by freeze-substitution or freeze-etching. *Cell Tissue Res.* 235: 225–241.

Menco, B. P. 1994. Ultrastructural aspects of olfactory transduction and perireceptor events. *Semin. Cell Biol.* 5:11–24.

Menco, B. P. 1997. Ultrastructural aspects of olfactory signaling. *Chem. Senses.* 22:295–311.

Menco, B. P., R. C. Bruch, B. Dau, and W. Danho. 1992. Ultrastructural localization of olfactory transduction components: the G protein subunit Golf alpha and type III adenylyl cyclase. *Neuron.* 8:441–453.

Menco, B. P. M., G. B. Birrell, C. M. Fuller, P. I. Ezeh, D. A. Keeton, and D. J. Benos. 1998. Ultrastructural localization of amiloride-sensitive sodium channels and Na^+, K^+-ATPase in the rat's olfactory epithelial surface. *Chem. Senses.* 23:137–149.

Mullins, L. J. 1977. A mechanism for Na/Ca transport. *J. Gen. Physiol.* 70:681–695.

Nakamura, T., and G. H. Gold. 1987. A cyclic nucleotide-gated conductance in olfactory receptor cilia. *Nature.* 325:442–444.

Nygren, A., and J. A. Halter. 1999. A general approach to modeling conduction and concentration dynamics in excitable cells of concentric cylindrical geometry. *J. Theor. Biol.* 199:329–358.

Pongracz, F., S. Firestein, and G. M. Shepherd. 1991. Electrotonic structure of olfactory sensory neurons analyzed by intracellular and whole cell patch techniques. *J. Neurophysiol.* 65:747–759.

Press, W. H., B. P. Flannery, S. A. Teukolsky, and W. T. Vetterling. 1990. Numerical Recipes in Pascal. Cambridge University Press, Cambridge, UK.

Qian, N., and T. J. Sejnowski. 1989. An electro-diffusion model for computing membrane potentials and ion concentrations in branching dendrites, spines and axons. *Biol. Cybern.* 62:1–15.

Rall, W. 1977. Core conductor theory and cable properties of neurons. *In* Handbook of Physiology, Section 1: The Nervous System. E. R. Kandel, editor. Oxford University Press, New York. 39–97.

Rasmusson, R. L., J. W. Clark, W. R. Giles, E. F. Shibata, and D. L. Campbell. 1990. A mathematical model of a bullfrog cardiac pacemaker cell. *Am. J. Physiol.* 259:H352–H369.

Reisert, J., and H. R. Matthews. 1998. Na^+-dependent Ca^{2+} extrusion governs response recovery in frog olfactory receptor cells. *J. Gen. Physiol.* 112:529–535.

Reuter, D., K. Zierold, W. H. Schröder, and S. Frings. 1998. A depolarizing chloride current contributes to chemoelectrical transduction in olfactory sensory neurons in situ. *J. Neurosci.* 18:6623–6630.

Schild, D., and D. Restrepo. 1998. Transduction Mechanisms in Vertebrate Olfactory Receptor Cells. *Physiological Reviews.* 78:429–466.

Sprott, J. C. 1991. Numerical Recipes, Routines and Examples in Basic. Cambridge University Press, Cambridge, UK.

Zufall, F., T. Leinders-Zufall, and C. A. Greer. 2000. Amplification of odor-induced Ca(2+) transients by store-operated Ca(2+) release and its role in olfactory signal transduction. *J. Neurophysiol.* 83:501–512.